IEEE International Conference on
"Nanomaterials: Applications & Properties" (NAP-2020)
Sumy, Ukraine, 9-13 Nov. 2020

Nanoscale Magnetic Properties of Additively Manufactured $FeCoNiAl_xMn_x$ High-Entropy Alloys

Anthoula Poulia
Department of Physics
University of Oslo
Oslo, Norway
anthoula.poulia@smn.uio.no

Calliope Bazioti
Department of Physics
University of Oslo
Oslo, Norway
kalliopi.bazioti@smn.uio.no

Spyros Diplas
SINTEF Industry
Oslo, Norway
Spyros.Diplas@sintef.no

Amin Azar
SINTEF Industry
Oslo, Norway
amin.azar@sintef.no

Branson Belle
SINTEF Industry
Oslo, Norway
Branson.Belle@sintef.no

Pavlo Mikheenko
Department of Physics
University of Oslo
Oslo, Norway
pavlo.mikheenko@fys.uio.no

Peter Svec
Institute of Physics
Slovak Academy of Sciences
Bratislava, Slovak Republic
peter.svec@savba.sk

Anette Eleonora Gunnæs
Department of Physics
University of Oslo
Oslo, Norway
a.e.gunnas@fys.uio.no

***Abstract*—Magnetic properties of High-Entropy Alloys based on the Fe-Co-Ni-Al-Mn system are reported. High-Entropy Alloys are cutting-edge technological materials containing five or more elements in relatively high concentrations (5–35 at.%) within one or several solid-state solutions. These solutions are stabilized at the nanometer scale due to the high contribution of the mixing entropy to the Gibbs free energy, which can overcome the enthalpic contribution. Two magnetic alloys are found in $FeCoNiAl_xMn_x$ (1.6 at.% ≤ x ≤ 7.8 at.%) samples processed by laser metal deposition. The magnetic techniques used to screen the materials were magneto-optical imaging and magnetic force microscopy. The former allows characterizing magnetic properties within the mm-µm scale, while the latter is efficient down to the nanometer scale. Magnetic screening confirms the importance of the nanostructure in defining magnetic properties of the alloys, and the trends in the magnetic behavior as a function of the alloy composition are revealed. The experimental results suggest that it is possible to form unique alloys, which may outperform conventional magnetic materials used in a variety of applications such as transformers, screening shields and wind power generators.**

Keywords—High-Entropy Alloys, magnetic properties, magneto-optical imaging, magnetic force microscopy, nano-structure

I. INTRODUCTION

High Entropy Alloys (HEAs) are an intensively investigated new class of metallic materials, which contain five or more elements mixed in nearly equal atomic proportions. HEAs ideally form simple solid solutions, stabilized by the thermodynamic balance between the mixing entropy and enthalpy of their constituent elements [1,2].

During their short period of exploration, many research efforts have been devoted to the investigation of the microstructural and mechanical properties [3,4] of these systems, while fewer works targeted their functional and magnetic properties.

HEAs are predicted to be good soft magnetic materials, with high saturation magnetization, low coercivity and good machinability [5,6]. However, the constituent elements, which can influence structural modifications and phase formation sequence and eventually impact magnetic properties, are difficult to select during the implementation of the alloy designing strategy [7].

In the above context, this study reports on the effect of compositional changes on the microstructural evolution and subsequently the magnetic properties of the produced HEAs.

II. EXPERIMENTAL DETAILS

A. *Preparation and characterization of the alloys*

$FeCoNiAl_xMn_x$ (1.6 at.% ≤ x ≤ 7.8 at.%) alloys were processed by Laser Metal Deposition (LMD) through weight controlled blending of elemental powder. The processing conditions and parameters were kept identical for all the samples. The microstructural characterization of the samples was performed using a TM3000 TableTop Scanning Electron Microscope, while the crystal structure of the bulk materials was analyzed with a Bruker D8 Advance diffractometer (Cu Kα, 40 kV 35 mA). Prior to all measurements the diffractometer was calibrated for 2 theta accuracy verification and for intensity accuracy verification using the NIST SRM1976 Al_2O_3 standard. The accuracy of determination of lattice parameters using total pattern analysis is better than 0.00002 nm. HighScore Plus was used for processing and fitting of the acquired diffraction patterns. No K_alpha2 stripping was performed prior to data evaluation. At the designing stage, various geometrical and thermodynamic parametric models were used as a first step of predicting the phase evolution in the system.

B. *Magneto-optical imaging*

Magneto-optical imaging (MOI) [8] was used as an express technique for monitoring magnetic properties of the materials. MOI is a technique that uses the Faraday Effect (rotation of the polarization angle of light in the presence of a magnetic film) in specially prepared indicator films, which, in this case, was in-plane magnetized bismuth-substituted ferrite garnet layer [9]. The indicator film, with a mirror on the bottom, is placed directly on the sample, and the incoming linear-polarized light beam crosses the film, reflects from the mirror, crosses it again and comes to the analyzer, which is directed at 90 degrees with respect to the polarizer used to produce polarized light. In the absence of magnetic field in the sample, there is no rotation of the polarization angle, and the beam does not pass the analyzer. The only areas that are seen in this technique are those that have a magnetic field. The higher the field – the brighter the beam that passes the analyzer. Since there is a mirror between the sample and the indicator film, the sample can only be seen if it is magnetic, in which case there is a change in the polarization of light in the film above.

C. *Magnetic force microscopy*

Magnetic force microscopy (MFM) [10-13] is another technique used in this work. It is a nanoscale technique allowing imaging magnetic properties of the samples with a magnetized tip, which is scanned above their surface. To distinguish between magnetic and van der Waals forces, which are also acting to the tip at small distances, a two-pass tapping mode scanning technique was recently developed [10,11]. In the first pass, topography close to the surface is measured at a tip oscillations frequency of about 74 KHz. In the next scan, the same topography is repeated at a fixed height above the surface. Above a certain height, which is typically 20 nm, van der Waals forces become weak, and pure magnetic response can be measured. During the scans, both the amplitude and phase of the oscillations are measured. According to theoretical analysis [10,12,13], the shift in the phase is proportional to the gradient of force acting to the tip. In the present study, measurements were done using two scanning probe microscopes: A Nanoscope at zero applied magnetic field and a JPK NanoWizard 4.0 in applied field of 0.58 T.

III. Results and Discussion

A. *Sample composition, evaluation of parametric models and structural features*

The nominal sample compositions are shown in Table I, together with selected thermodynamic and geometric parameters extracted from the literature [14-16]. It is suggested that single solid solution phase formation requires the following conditions (among others) to be met:

i) The valence electron concentration (VEC) must be below 6.78 for the formation of stable face centered cubic (FCC) phases, or above 8 for the formation of body centered cubic (BCC) phases [14].

ii) The atomic size parameter (γ), which takes into consideration the atomic packing misfit in multicomponent systems, should be below 1.175, to satisfy a limit condition for achieving simple solid solution [15].

iii) The parameter Φ should be above 1 for the formation of a stable solid solution. Φ is defined as $\Phi=\Delta G_{ss}/-|\Delta G_{max}|$, where ΔG_{ss} is the change in Gibbs free energy for the formation of a fully disordered solid solution from a mixture of its individual elements and ΔG_{max} is the lowest (intermetallic) or highest (segregated) possible Gibbs free energy obtainable from the formation of binary systems from the constituents of the mixture. Negative Φ values indicate that solid solution will not be formed, owing to positive formation enthalpy [16].

The calculated values of the above-mentioned parameters for the nominal compositions listed in Table I, suggest that all samples will have a phase separation tendency rather than forming a single solid solution. In particular, samples A-D are predicted to form both BCC and FCC phases, while the rest of the samples should mainly contain FCC phases.

TABLE I. Nominal Elemental Content of the Produced HEAs and their Main Parameters Calculated according Prediction Models [14 – 16]

Sample code	*Element content (at.%)*	*VEC [14]*	*γ [15]*	*Φ [16]*
A	$Fe_{28.1}Co_{28.1}Ni_{28.1}Al_{7.8}Mn_{7.8}$	8.367	1.1705	0.312
B	$Fe_{28.8}Co_{28.8}Ni_{28.8}Al_{6.8}Mn_{6.8}$	8.456	1.1706	0.300
C	$Fe_{29.4}Co_{29.4}Ni_{29.4}Al_{5.9}Mn_{5.9}$	8.528	1.1707	0.289
D	$Fe_{29.6}Co_{29.6}Ni_{29.6}Al_{5.6}Mn_{5.6}$	8.552	1.1708	0.286
E	$Fe_{31.6}Co_{31.6}Ni_{31.6}Al_{2.6}Mn_{2.6}$	8.792	1.1713	0.248
F	$Fe_{32.3}Co_{32.3}Ni_{32.3}Al_{1.6}Mn_{1.6}$	8.881	1.1714	0.235

X-ray diffraction (Fig. 1) indicates that samples A-D are dominated by a mixture of FCC and BCC phases with a = 3.6092 Å and a = 2.892 Å, respectively. Samples E and F have diffraction peaks consistent with a solid solution single-phase FCC with a = 3.5969 Å and a = 3.5959 Å, respectively. It should be noted that the relative peak intensity ratios between the FCC reflections (like I_{111}/I_{200}) change dramatically from sample A to F, where the intensity profiles of E and F is closest to what can be expected for the A1 type of FCC structure with space group Fm-3m. Preliminary data from TEM indicate a more complex nanostructure. With SEM and TEM, additional phases are observed, but the volume is low and cannot be detected in the current XRD analysis. All these phases are magnetic, as was proved by the magnetic screening techniques.

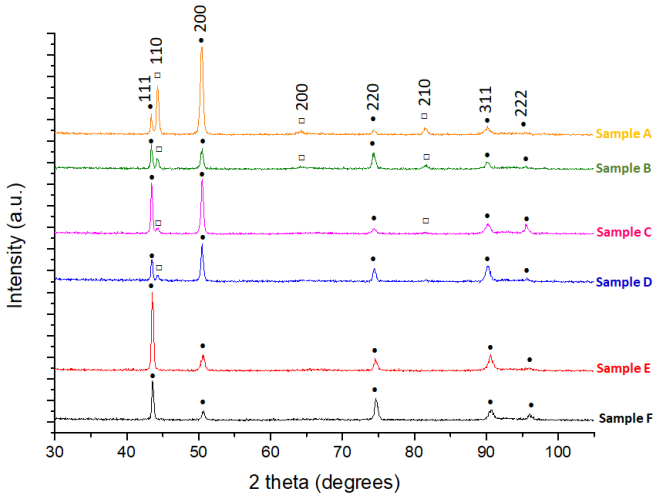

Fig. 1. XRD patterns of the as-cast $FeCoNiAl_xMn_x$ HEAs (• FCC (Fm-3m), □ BCC (Im-3m)).

Regarding their microstructural features, the samples show a dendritic morphology rich in Fe, Co and Ni and the interdendritic areas rich in Al and Mn. The samples containing the highest atomic percentages of Al and Mn (Fig 2a-c) are characterized by large dendrites (light grey) and a reduced interdendritic fraction (dark grey). Some dark Al-Mn oxidized inclusions are also spotted at the interface between the two regions. Gradually, due to alterations in the solidification mechanism (e.g. variations in temperature gradient and/or critical growth velocity), the microstructure of the samples with the lower Al and Mn contents (Fig. 2d-f) turns into more cellular configurations, where the dark inclusions, rich in Al-Mn, seem to increase.

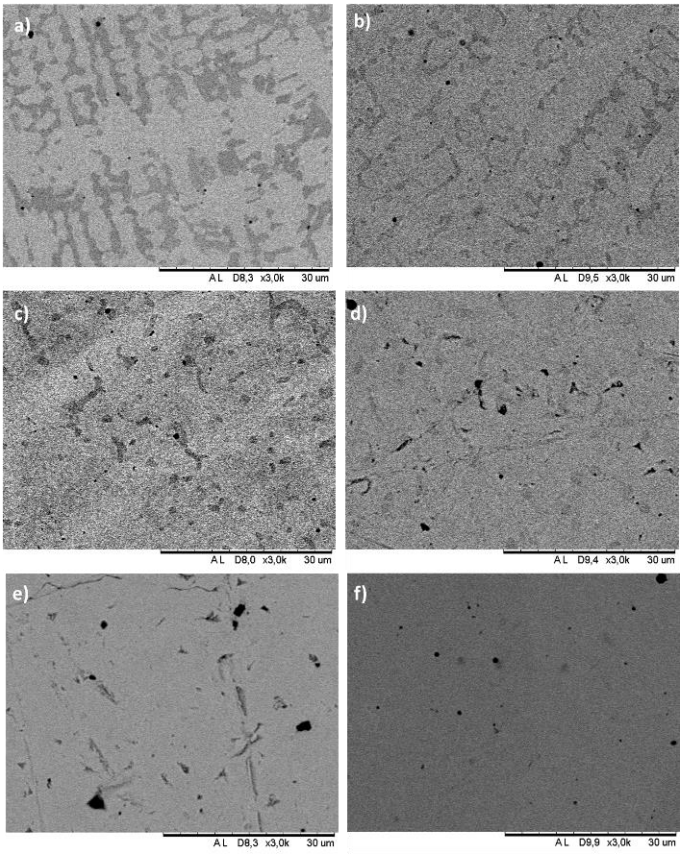

Fig. 2. Backscattered electron SEM micrographs of the as-cast $FeCoNiAl_xMn_x$ HEAs (a - f: Sample A - Sample F).

B. Low-field behavior of HEA

The micro and nanoscale features observed in the structural study are reflected in the magnetic properties of the alloys. One can distinguish between low and high-field behavior of the samples.

The low-field magnetic behavior of the samples is revealed by magneto-optical (MO) imaging, which is typically working in magnetic fields up to 100 mT. As an example, Fig. 3 shows the MO image of sample A recorded in a magnetic field of 26.86 mT. The sample is behind the MO indicator film outlined by straight lines close to top corners of the frame.

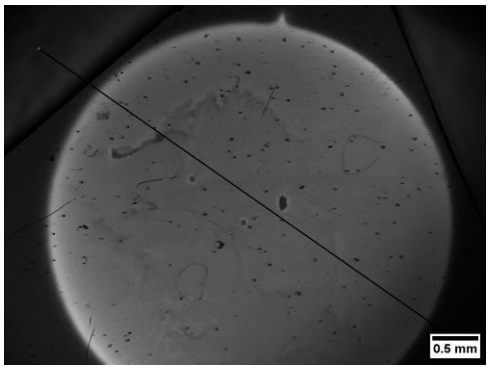

Fig. 3. Magneto-optical image of Sample A at a magnetic field of 26.86 mT revealed behind the indicator film. The large domains with slightly differently magnetization are evident in the sample.

Fig. 4 shows a line profile of the intensity of the light in the sample shown in Fig. 3.

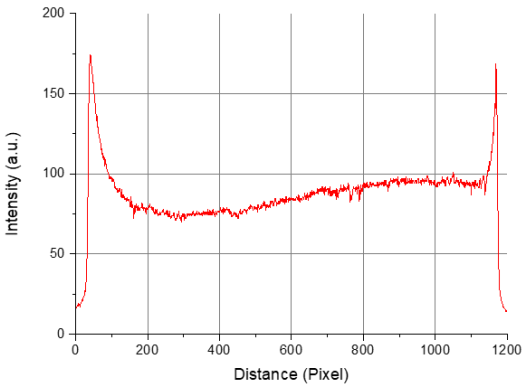

Fig. 4. A line profile of the intensity of the light in the sample shown in Fig. 3. The position of the peaks in the intensity corresponds to the edges of the sample.

Similar images and line profiles were recorded for all samples at different applied magnetic fields. An interesting feature is that MOI reveals magnetic state of the samples also at zero applied field. This means that there is a spontaneous magnetization in the sample and/or it is magnetized by the magnetic field of the Earth. The measured intensity of magnetization is reversible upon the application of a magnetic field, i.e. it is the same when increasing or decreasing the magnetic field up to a value of 27 mT. In other words, the coercivity of the material is below the detection level of the technique. The low coercivity is a useful property for soft magnetic materials, which ensures the absence of considerable hysteresis losses during the re-magnetization of the samples. This can make the materials suitable for a range of practical applications.

An important property of the profile in Fig. 4 is the presence of sharp peaks close to the edges of the sample. These peaks are attributed to the demagnetizing factor of the cylindrical samples behind the MO film. The height and sharpness of the peaks depend on the magnetic susceptibility of the sample [17]. The peaks observed here indicate a high value of magnetic susceptibility, which, again, is useful for practical magnetic applications.

A careful look at MO images also reveals large domains with slightly different magnetization. These domains correspond to differently oriented grains of the main phase, as seen in the microstructural images. Such magnetic

anisotropy is not useful for applications, but it is not strong, and its influence could further be minimized by a thermal treatment aiming to reduce the size of the domains.

The comparison of the low-field magnetic properties of the alloys presented in Table I by using MO images and their line profiles similar to those shown in Figs. 3 and 4, allowed to conclude that the magnetic properties of all samples are similar, but the highest average magnetization is achieved in samples B and F.

C. Magnetic behavior of the samples revealed by MFM scans

The MFM sheds light on mainly high-field magnetic behavior of the samples. Although MFM scans were also recorded in zero applied field, the material tends to be magnetized by the strong field of MFM tip. The MFM scans obtained with the application of a large external magnetic field are typically of better contrast than those recorded in zero field. As such, the interesting features of MFM scans obtained here include a homogeneous stripy domain structure in Sample E and inclusions with such domain structure in Sample B. Other samples show irregular magnetic structure with magnetic domains of different sizes and shapes. The presence of nano-sized magnetic grains is common in all samples and strongly influences their large-scale magnetic behavior.

Fig. 5 presents a homogeneous in-field stripy domain structure in Sample E, and the fragments of such a structure in Sample B. Similar fragments are observed in zero magnetic field in Sample A, giving an evidence of its spontaneous magnetization.

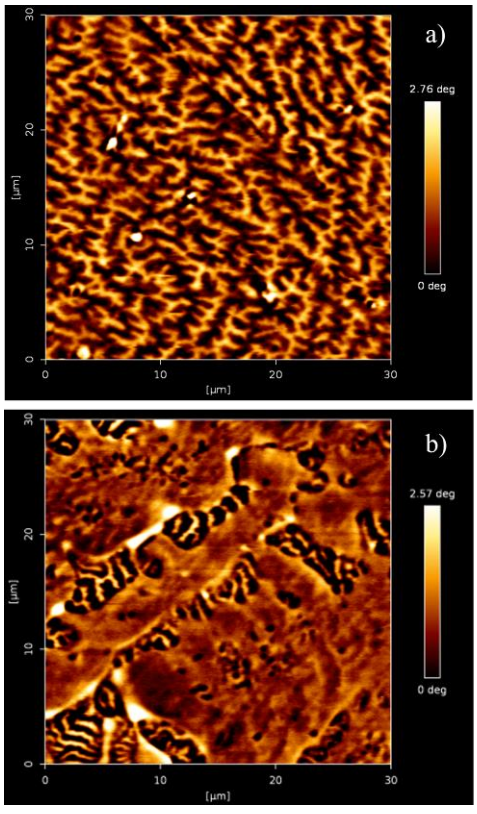

Fig. 5. a) MFM image of sample E showing homogeneous stripy domain structure. b) Fragments of stripy domain structure in sample B.

Finally, Fig. 6 shows a strongly magnetic (dark color) individual nanoparticle in Sample F. Smaller nanoparticles around it show weaker magnetism or even interact repulsively with the tip.

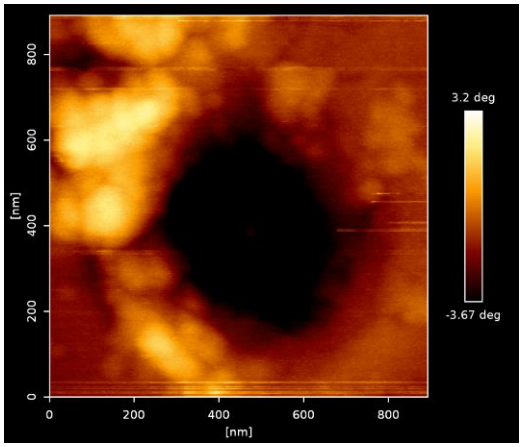

Fig. 6. MFM image of an individual magnetic nanoparticle in Sample F. Dark color, or negative phase shift, demonstrates attraction of nanoparticle to the tip.

IV. CONCLUSIONS

Magnetic characterization was performed on a selective number of $FeCoNiAl_xMn_x$ HEA alloys. An initial attempt to predict their phase evolution was supported by the literature parametric models, while their actual crystal structure and microstructural features were also evaluated. The alloys consisted of FCC and BCC phases, or a single FCC phase with the lowest atomic percentage of Al and Mn. Their microstructure was mainly dendritic, with a transition to more cellular configuration, as the atomic percentage of Al and Mn was decreasing. In terms of magnetic properties, the samples showed a spontaneous magnetization, as was confirmed by both MOI and MFM, while their low coercivity, evident from MOI, ensures the absence of considerable hysteresis losses during the re-magnetization and classifies them as appropriate candidates for soft magnetic applications. MFM scans revealed either homogeneous stripy domain structure accompanied by some inclusions or irregular magnetic structure, in which magnetic domains were of different sizes and shapes. Finally, nano-sized magnetic grains, which influence the sample's large-scale magnetic behavior were detected.

ACKNOWLEDGMENT

This work is part of the Project "MAGNIFICENT - Additively manufactured magnetic high entropy alloys for renewable electricity", funded by the Research Council of Norway (pr. nr 287979) within the Nano2021 Program.

REFERENCES

[1] Y.F. Ye, Q. Wang, J. Lu, C.T. Liu and Y. Yang, "High-entropy alloy: challenges and prospects," Materials Today, vol. 19, Number 6, pp. 349-362, July-August 2016.

[2] E.P. George, D. Raabe and R.O. Ritchie, "High- entropy alloys," Nature Reviews | Materials, vol. 4, pp. 515-534, August 2019.

[3] P. Shi, W. Ren, T. Zheng, Z. Ren, X. Hou, J. Peng, P. Hu, Y. Gao, Y. Zhong and P.K. Liaw, "Enhanced strength–ductility synergy in ultrafine-grained eutectic high-entropy alloys by inheriting microstructural lamellae," Nat. Commun., vol. 10, pp. 489, January 2019.

[4] Y.Y.Liu, Z. Chen, J.C. Shi, Z.Y. Wang and J.Y. Zhang, "The effect of Al content on microstructures and comprehensive properties in $Al_xCoCrCuFeNi$ high entropy alloys," Vacuum, vol 161, pp. 143-149, March 2019.

[5] R.K. Mishra and R.R. Shahi, “Novel $Co_{35}Cr_5Fe_{20}Ni_{20}Ti_{20}$ high entropy alloy for high magnetization and low coercivity,” J. Magn. Magn. Mater., vol. 484, pp. 83-87, August 2019.

[6] T. Zuo, X. Yang, P.K. Liaw and Y. Zhang, “Influence of Bridgman solidification on microstructures and magnetic behaviors of a non-equiatomic FeCoNiAlSi high-entropy alloy,” Intermetallics, vol 67, pp. 171-176, December 2015.

[7] R.F. Zhao, B. Ren, G.P. Zhang, Z.X. Liu and J.J. Zhang, “Effect of Co content on the phase transition and magnetic properties of $Co_xCrCuFeMnNi$ high-entropy alloy powders,” J. Magn. Magn. Mater., vol. 468, pp. 14-24, December 2018.

[8] T.H. Johansen and D.V. Shantsev, (Ed.), Magneto-Optical Imaging, Dordrecht: Kluwer Academic Publishers, 2004, pp. 1-345.

[9] L.E. Helseth, R.W. Hansen, E.I. Il'yashenko, M. Baziljevich, and T.H. Johansen, “Faraday rotation spectra of bismuth-substituted ferrite garnet films with in-plane magnetization,” Phys. Rev. B, vol. 64, 174406, October 2001.

[10] D. Passeri, C. Dong, M. Reggente, L. Angeloni, M. Barteri, F.A. Scaramuzzo, F. De Angelis, F. Marinelli, F. Antonelli, F. Rinaldi, C. Marianecci, M. Carafa, A. Sorbo, D. Sordi, I. WCE Arends, and M. Rossi, “Magnetic force microscopy. Quantitative issues in biomaterials,” Biomatter, vol. 4, e29507, July 2014.

[11] G. Cordova, B.Y. Lee, and Z. Leonenko, “Magnetic Force Microscopy for Nanoparticle Characterization,” NanoWorld Journal, vol 2, pp. 10-14, April 2016.

[12] B. Torre, G. Bertoni, D. Fragouli, A. Falqui, M. Salerno, A. Diaspro, R. Cingolani, and A. Athanassiou, “Magnetic, force microscopy and energy loss imaging of superparamagnetic iron oxide nanoparticles,” Sci. Rep., vol.1, 202, December 2011.

[13] Sarid D, Scanning Force Microscopy. New York, USA: Oxford University Press, 1994.

[14] S. Guo and C.T. Liu, “Phase stability in high entropy alloys: Formation of solid-solution phase or amorphous phase,” Prog. Nat. Sci., vol 21, pp. 433-446, December 2011.

[15] Z. Wang, Y. Huang, Y. Yang, J. Wang and C.T. Liu, “Atomic-size effect and solid solubility of multicomponent alloys,” Scripta Mater., vol 94, pp. 28-31, January 2015.

[16] D.J.M. King, S.C. Middleburgh, A.G. McGregor and M.B. Cortie, “Predicting the formation and stability of single phase high-entropy alloys,” Acta Mater., vol 104, pp. 172-179, February 2016.

[17] D.X. Chen and J.A. Brug, “Demagnetizing Factors for Cylinders,” IEEE Transactions on Magnetics, vol. 21, pp. 3601-3619, July 1991.